






Next-nearest-neighbor coupling with spinor polariton condensates

Dmitriy Dovzhenko ^{1,*}, Denis Aristov ¹, Lucinda Pickup ¹, Helgi Sigurðsson ^{2,3} and Pavlos Lagoudakis ^{1,4}

¹*School of Physics and Astronomy, University of Southampton, Southampton SO17 1BJ, United Kingdom*

²*Science Institute, University of Iceland, Dunhagi 3, IS-107 Reykjavik, Iceland*

³*Institute of Experimental Physics, Faculty of Physics, University of Warsaw, ul. Pasteura 5, PL-02-093 Warsaw, Poland*

⁴*Hybrid Photonics Laboratory, Skolkovo Institute of Science and Technology, Territory of Innovation Center Skolkovo, Bolshoy Boulevard 30, building 1, 121205 Moscow, Russia*



(Received 12 January 2023; revised 15 May 2023; accepted 15 September 2023; published 11 October 2023)

We report on experimental observation of next-nearest-neighbor coupling between ballistically expanding spinor exciton-polariton condensates in a planar semiconductor microcavity. All-optical control over the coupling strength between neighboring condensates is demonstrated through distance-periodic pseudospin screening of their ballistic particle outflow due to the inherent splitting of the planar cavity transverse-electric and transverse-magnetic modes. By screening the nearest-neighbor coupling we overcome the conventional spatial coupling hierarchy between condensates. This offers a promising route toward creating unconventional nonplanar many-body Hamiltonians using networks of ballistically expanding spinor exciton-polariton condensates.

DOI: [10.1103/PhysRevB.108.L161301](https://doi.org/10.1103/PhysRevB.108.L161301)

Strongly correlated quantum many-body systems have attracted a lot of interest as a promising tool to engineer and explore phases of matter in extreme settings [1–3] and to simulate complex Hamiltonians [4,5]. Such systems include ultracold-atomic ensembles [4], trapped ions [6,7], nuclear and electronic spins [8,9], superconducting circuits [10,11], and nonlinear photonic systems [12]. Of interest, recent milestone achievements in programmable connectivity in condensed matter using cold-atomic gases [13] now permit construction of intriguing networks of coupled elements. However, in general, many laboratory systems are by their physical nature unable to form unconventional graph topologies. In the past decade, driven-dissipative Bose-Einstein condensates of exciton-polaritons (from here on, polaritons) in planar microcavities have substantially advanced in optical reprogrammability [14–21]. There, each condensate is driven by a focused nonresonant optical excitation beam forming a localized macroscopically coherent wave function [22]. The coupling strength between neighboring condensates is roughly given by their mutual overlap with an exponential fall-off as a function of separation distance [23–25]. This means that nearest-neighbor (NN) coupling dominates over next-nearest-neighbor (NNN) coupling, making polariton networks inherently planar in a graph topology sense. Overcoming this spatial coupling hierarchy can offer opportunities to observe spontaneous ordering and emergent polariton effects in nonplanar graph topologies [26–32]. However, this

is extremely challenging, requiring very fine control over the two-dimensional polariton potential landscape with limitations of its own [33].

In this Letter, we demonstrate that spin-orbit coupled (SOC) exciton-polariton condensates can overcome this challenge. Polaritons are quasiparticles exhibiting intermixed properties of excitons and photons, which appear when light and matter are brought to the strong-coupling regime [34]. As a consequence, the photon polarization is explicitly connected to the polariton pseudospin (or just “spin” for short) with $\hat{\sigma}_z = \pm 1$ spin projections along the cavity growth axis representing σ^\pm circularly polarized light. Their two-component integer spin structure has led to deep exploration into nonequilibrium spinor quantum fluids [35]. Polaritons mostly decay through photons leaking out of the cavity containing all the information on the condensate such as energy, momentum, density, and spin. This salient feature allows direct, yet nondestructive, measurement of the condensate spin distribution using polarization resolved photoluminescence (PL) imaging.

Both the polariton condensate and the incoherent photoexcited background of excitons sustaining it adopt the circular polarization of the nonresonant excitation [36,37] due to the optical orientation effect of excitons [38,39] and spin-preserving stimulated scattering of excitons into the condensate [40]. This permits excitation of a condensate of a well-defined macroscopic $S_z \sim \langle \hat{\sigma}_z \rangle$ spin projection [41–44]. Subsequently, the inherent transverse electric–transverse magnetic (TE-TM) splitting of the microcavity [45] will start rotating the spin of any condensate polaritons which obtain finite wave vector and flow away from the pump spot [46,47]. This is also referred to as the optical spin Hall effect [48,49]. Namely, the splitting between TE and TM polarized cavity photon modes acts as a directionally dependent in-plane effective magnetic field [48,50] (i.e., effective SOC [51]) causing the spins of outflowing condensate polaritons to start

*DovzhenkoDS@gmail.com

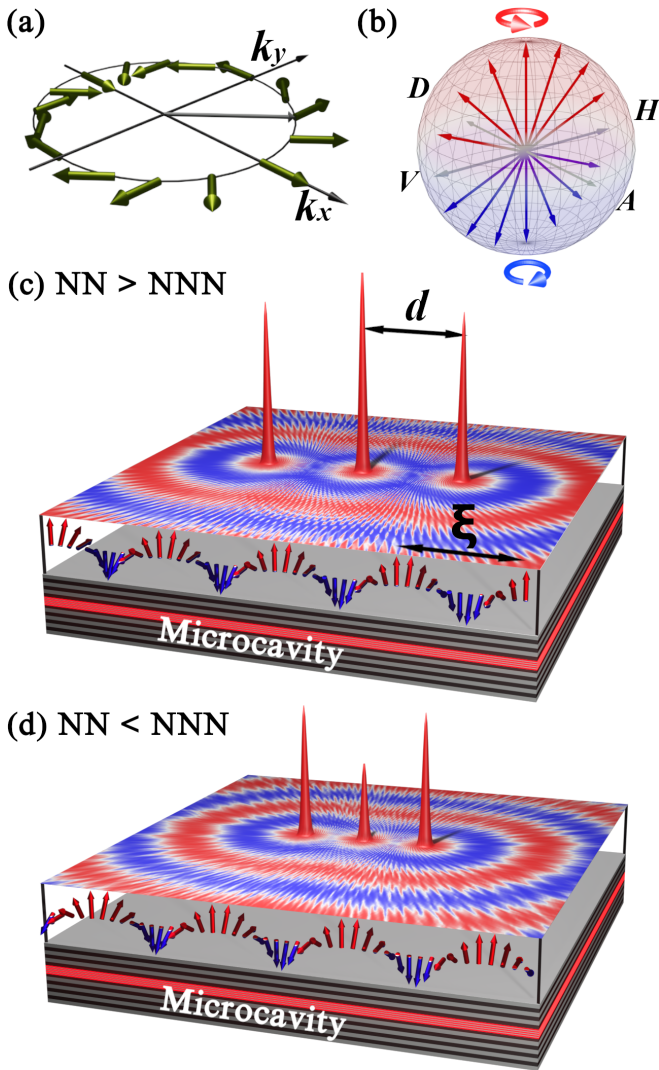


FIG. 1. (a) Schematic of the effective SOC magnetic field distribution (dark olive arrows) from the TE-TM splitting on a momentum-space circle. (b) Schematic of the Poincaré sphere showing example pseudospin precession as polaritons propagate (blue and red arrows). Schematic representing two pump geometries where the distance between the central and edge pump spots equals (c) one full period of pseudospin oscillation (NN is stronger than NNN) and (d) half oscillation period (NN is weaker than NNN). The height of the peaks represents the intensity of the condensate emission, and the red, white, and blue color map shows the precession of the polariton pseudospin propagating in the cavity plane, with red representing $S_z = +1$ (spin-up polaritons) and blue representing $S_z = -1$ (spin-down polaritons). Red and blue arrows show the pseudospin precession of the polaritons propagating from the edge condensates along the triad axis.

precessing [see Fig. 1(a) and Fig. 1(b)]. The strength of this effective SOC scales quadratically with the polariton momentum, $\propto k^2$, and can even be electrically tuned [52,53]. This makes so-called ballistic condensates ideal for enhanced SOC effects [46,47] due to their extremely high kinetic energies obtained through repulsive Coulomb interactions with the locally pump-induced exciton reservoir. Moreover, because of their long-range coherent particle outflow, ballistic con-

densates can couple over macroscopic distances much greater than their respective full width at half maximum [24] while also preserving their spin information [44,46,47].

Recently, it was theoretically predicted that ballistic condensates could invert their neighbor coupling hierarchy, making NNN stronger than NN, through a spin-screening effect made possible by the effective SOC stemming from TE-TM splitting [54]. Here, we provide experimental evidence of these recent predictions. We present a study of a spinor polariton dyad (two coupled condensates) and a triad [three coupled condensates; see schematic Fig. 1(c)] wherein each condensate ballistically emits a coherent pseudospin current which rapidly precesses as it propagates [46,47]. We demonstrate control over the coupling strength between neighboring condensates by changing the spatial distance between them (denoted d) relative to the spatial precession period of the condensate pseudospin (denoted ξ).

We briefly explain the idea of spin-screened polariton coupling. The three peaks in Fig. 1(c) represent the condensate centers excited by three co-localized Gaussian pump spots of equal intensity. The red-blue color map shows the precession of the polariton pseudospin as it radially propagates in-plane away from each condensate center, with red representing $S_z = +1$ (spin-up polaritons) and blue representing $S_z = -1$ (spin-down polaritons). The height of the peaks represents the intensity of the condensate emission. The distance between the condensate centers relative to the spatial oscillations of the pseudospin modifies the coupling between them. In the nonscreened state [Fig. 1(c)] NN condensates are excited at a distance equal to integer number of periods of pseudospin oscillations, $d = n\xi$ where $n = 1, 2, 3, \dots$. This means that propagating condensate polaritons arrive at NNs with unchanged spin projection. On the contrary, in the screened state [Fig. 1(d)] NNs are separated by $d = (n - 1/2)\xi$ and polaritons arrive at their NNs with opposite spin projection which reduces the condensate coupling, while coupling between NNNs is still maintained.

The microcavity used in this study consists of a $5\lambda/2$ AlGaAs cavity surrounded by two distributed Bragg mirrors (DBRs) of 35 and 32 pairs of AlGaAs/AIAs for the bottom and top DBRs correspondingly with the 12 GaAs quantum wells separated into four sets of three quantum wells placed at the antinodes of electric field within the cavity. The cavity quality factor is around $Q \sim 16000$ with the corresponding polariton lifetime $\tau_p \approx 5$ ps and Rabi splitting of 9 meV. The measured TE-TM splitting is ≈ 0.2 meV at $k = 3 \mu\text{m}^{-1}$ in-plane wave vector. The microcavity had the same detuning in all pumping spot positions providing equal values of the condensation threshold for each single isolated condensate. See Sec. S1 in the Supplemental Material [55] for further experimental details.

The normalized Stokes parameters of the cavity emission are written

$$S_{x,y,z}(\mathbf{r}) = \frac{I_{H,D,\sigma^+}(\mathbf{r}) - I_{V,A,\sigma^-}(\mathbf{r})}{I_{H,D,\sigma^+}(\mathbf{r}) + I_{V,A,\sigma^-}(\mathbf{r})}, \quad (1)$$

where $\mathbf{r} = (x, y)$ is the in-plane coordinate and $I_{H(V),D(A),\sigma^+(\sigma^-)}(\mathbf{r})$ corresponds to horizontally (vertically), diagonally (antidiagonally), and right-circularly (left-circularly) polarized (RCP and LCP for short) PL, respectively. Formally,

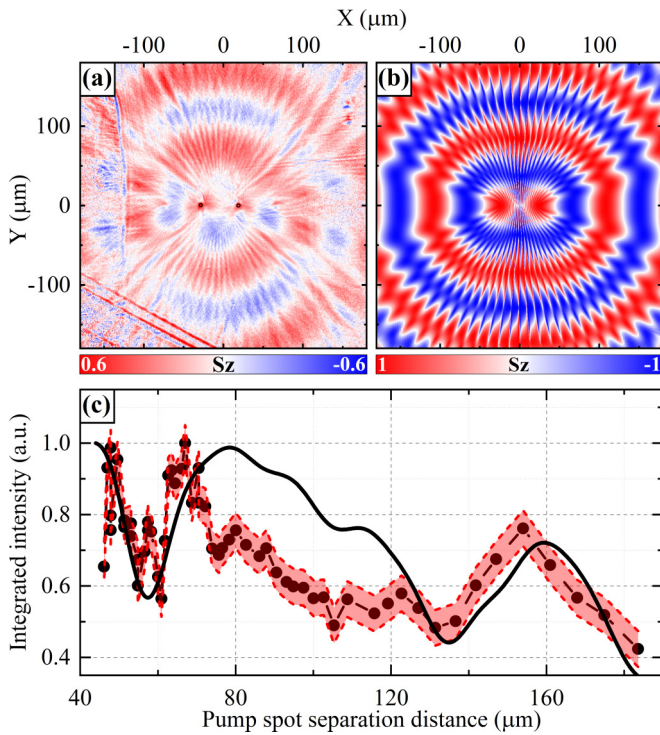


FIG. 2. Two polariton condensates. (a) Experimentally measured and (b) simulated numerically real-space S_z component of the Stokes vector of the polariton condensate emission. In panel (a) black circles show the position of pump spots. (c) Total integrated emission intensity dependence on the separation distance between two condensate pump spots. In panel (c) black dots show the experimentally measured values with red region representing the error of the total intensity value. Black curve shows the same dependence calculated numerically.

the Stokes parameters relate to the condensate pseudospin through $\mathbf{S} = \langle \Psi^\dagger | \hat{\sigma} | \Psi \rangle / \langle \Psi^\dagger | \Psi \rangle$, where $\Psi = (\psi_+, \psi_-)^T$ is the condensate spinor order parameter and $\hat{\sigma}$ is the Pauli matrix vector. The $S_x(\mathbf{r})$ and $S_y(\mathbf{r})$ components represent the degree of linear and diagonal polarization but are not important in this study (also due to the predominant circular polarization of the condensates used here). Experimental measurements were reproduced using a generalized two-dimensional Gross-Pitaevskii equation (2DGPE) (see Sec. S2 in the Supplemental Material [55] with Refs. [56,57] therein).

In Fig. 2 we present results for two polariton condensates separated by $d \approx \xi/2$. Data for a single isolated condensate give a S_z period around $\xi \approx 90 \mu\text{m}$ (see Sec. S1 in the Supplemental Material [55]). Figures 2(a) and 2(b) show the measured and simulated spatial distribution of the S_z component with spatial pseudospin oscillations clearly visible due to the SOC rotating the spin of the outflowing polaritons. Note that unavoidable dephasing of polaritons in experiment results in lowered S_z values compared to simulations as indicated on the color bars. Smaller ripple-like modulations are also visible due to the standing wave interference between the two phase-locked condensates as reported before [24,44,54]. These ripples are characterized by a small-scale period $\lambda = 2\pi/\langle k_c \rangle \approx 3 \mu\text{m}$, where $\langle k_c \rangle$ is the average outflow momentum of polaritons from their condensates. In contrast, the

large-scale S_z period is given by $\xi = 2\pi/\Delta_k \gg \lambda$, where $\hbar\Delta_k/\sqrt{2\varepsilon_c} = |\sqrt{m_{\text{TE}}} - \sqrt{m_{\text{TM}}}|$ and $\varepsilon_c \approx 3 \text{ meV}$ is the condensate energy (measured from $k = 0$ at the dispersion), and $m_{\text{TE, TM}}$ are the effective masses of TE and TM polarized polaritons [45].

The spin-screening effect can be observed as periodic extrema in the integrated PL intensity, which represents the condensate occupation, as a function of separation distance d in Fig. 2(c). At the maxima the coupling is unscreened and NN coupling is strong. At the minima the coupling is screened and NN coupling is weak. Black dots and the black solid curve denote experimental measurements and calculations, respectively. In the absence of SOC one would observe monotonically decreasing emission intensity with only short variations (order of λ) corresponding to in-phase and antiphase flip-flop transitions between the synchronized condensates [24]. Instead, we observe strong nonmonotonic behavior with clearly visible maxima around 67 and 154 μm , and minima around 56 and 135 μm . Notice that the distance between the two maxima and the two minima correlates with the measured $\xi \approx 90 \mu\text{m}$ period of S_z oscillations.

The discrepancy between the absolute locations of the minima and maxima with the predicted critical distances for screened ($\xi/2, 3\xi/2$) and unscreened ($\xi, 2\xi$) coupling, respectively, can be understood as follows. First, when two condensates are coupled their energy is redshifted on average [24] leading to smaller ε_c and thus larger ξ in the coupled system. Second, the finite width of the pump spots modulates the phase of polaritons and causes a shift in the S_z period. Third, the cavity here has higher levels of disorder than strain-compensated cavities [58] which can affect the spatial coupling. That is why the relative distances between the extrema are more meaningful than their absolute locations. This interpretation is verified in 2DGPE modeling which accurately reproduces the locations of the extrema. Note that the slight discrepancy between modeling and experiment in Fig. 2(c) between 70 and 120 μm can possibly be attributed to the large parameter space of the 2DGPE making quantitative matching somewhat challenging or localized defects in the sample which scatter outflowing polaritons, consequently decreasing the coupling efficiency. Indeed, the integrated emission intensity of the coupled condensate system is proportional to their non-Hermitian coupling strength from their mutual overlap over the pumped areas, since it determines both the imaginary (and real) part of their complex energies [23]. However, large defects are scarce in the sample [46]. In order to verify that the modulation we observe is dominantly coming from the spin-screening effect we have carefully chosen a clean part of the sample, with the minimum amount of large defects. We also tested a few other relatively clean sample locations and found qualitatively the same modulation period in the integrated emission dictated by the period of the spin precession.

In order to demonstrate the NNN coupling using the all-optical spin-screening effect we investigated the system containing a chain of three condensates similar to the system depicted schematically in Fig. 1. As in the previous experiment with two condensates, all condensates were excited using tightly focused RCP laser pump spots of equal intensity above threshold. Figures 3(a) and 3(b) show the measured

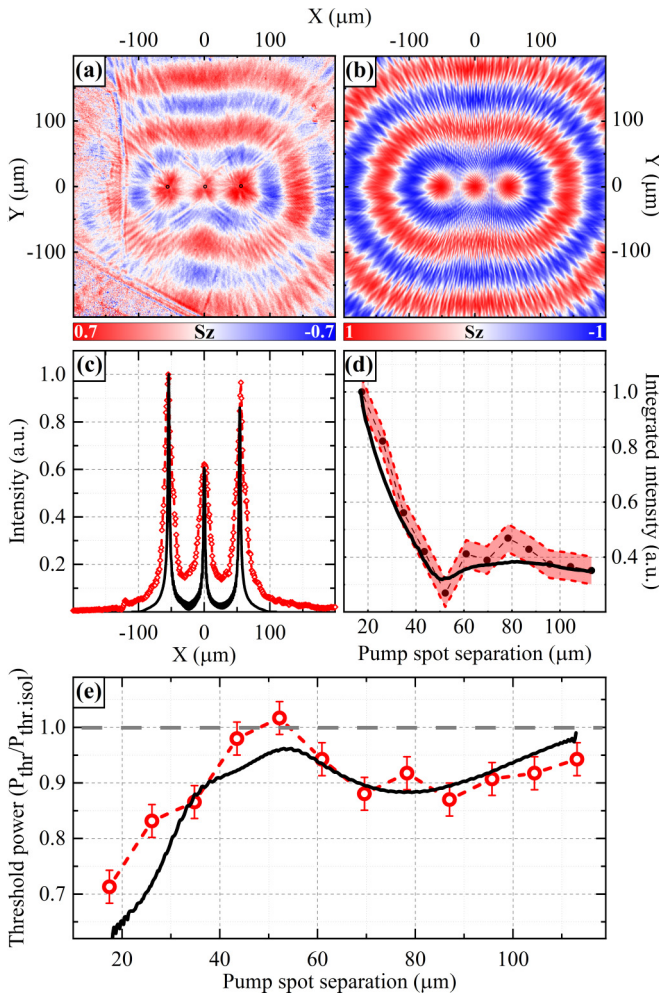


FIG. 3. Three polariton condensates. (a) Experimentally measured and (b) simulated real-space S_z component of the Stokes vector of the polariton condensate emission. In panel (a) black circles show the position of pump spots. (c) Measured experimentally (red diamonds) and calculated numerically (solid black curve) real-space intensity distribution along the triad axis. (d) Dependence of the central condensate PL intensity on the separation distance between the condensate pump spots measured experimentally (black dots) and calculated numerically (solid black curve); red region represents the error of the total intensity value. The dashed curves are guides to the eye. (e) The system threshold power dependence on the separation distance between the condensate pump spots measured experimentally (red circles) and calculated numerically (solid black curve); red bars represent the error. Gray dashed line in panel (e) shows the threshold power for single isolated condensate.

and simulated spatial distribution of the three-condensate S_z component with NN distance of $d \approx \xi/2$. As in the previous case of two condensates, the system forms a joint macroscopic coherent state resulting in an oscillating S_z pattern elongated along the horizontal axis with three RCP condensate circles of equal degree of polarization in the center. Amazingly, the intensity of the central condensate was suppressed relative to the outer ones, evidencing reduced NN coupling due to the spin-screening effect; see in Fig. 3(c) measured (red diamonds) and simulated (black solid curve) intensity distribution along the triad axis.

To unambiguously demonstrate the spin-screening effect in the triad, we measured (dots) and simulated (solid curve) the dependence of the central condensate intensity as a function of NN separation distance with results presented in Fig. 3(d). Both experiment and calculations show a clear dip around $d = 52 \mu\text{m} \approx \xi/2$, corresponding to spin-screened NN coupling, followed by a small peak around $d = 80 \mu\text{m} \approx \xi$ where the NN coupling is restored. The observed suppression of the central condensate intensity provides strong evidence of spin-screened NN coupling mediated by the spin coherence of the system.

Moreover, we experimentally measured pump power dependence for each separation distance and extracted polariton condensation threshold values, which are shown in Fig. 3(e) (red circles). The horizontal dashed line is the threshold value of the isolated condensate. In the absence of the TE-TM splitting, monotonic increase of the threshold value converging to the isolated condensate threshold is expected with the increase of the separation distance between the condensates. In our system we observe the maximum threshold at the separation distance of $52 \mu\text{m}$, which precisely corresponds to the minimum of the central condensate intensity in Figs. 3(c) and 3(d). This confirms that the NN condensate interaction is effectively screened at this separation distance due to the TE-TM splitting. Around a separation distance close to the full period of S_z oscillation ($d \approx \xi$) a decrease in the threshold power was observed, as expected with NN coupling restored. A simple linear coupled oscillator model [solid curve in Fig. 3(e)] is able to explain the behavior of the threshold power (see Sec. S3 in the Supplemental Material [55]).

In summary, we have experimentally demonstrated that next-nearest-neighbor coupling can be made stronger than nearest-neighbor coupling in ballistically expanding spinor exciton-polariton condensates which was recently proposed in Ref. [54]. This unconventional near-inversion of the spatial coupling hierarchy between condensates stems from the combination of TE-TM splitting and the ballistic polariton flow from each condensate. Outflowing polaritons experience effective spin-orbit coupling which rotates their spin state as they propagate from one condensate to the next. Depending on distance, the overlap (coupling) between the condensates can become spin screened depending on the polariton spin projection upon arrival at its neighbor. We believe that the demonstrated alteration of the conventional condensate coupling hierarchy could pave the way toward all-optical simulation of many-body ballistic systems belonging to nonplanar graph topologies using networks of spinor polariton condensates. In particular, we have noticed a resemblance between the distance-dependent spinor polariton condensate coupling strength and the well-known RKKY mechanism (see Sec. S4 in the Supplemental Material [55] with reference [59] therein), which offers perspectives on polaritonic simulation on long-range coupled magnetic dipoles in conductive materials. Another, intriguing effect of making NN polariton coupling strength comparable to NNN couplings in square graphs is the potential to generate stable array vortices through XY energy minimization [21] (see Sec. S5 in the Supplemental Material [55] with Ref. [32] therein).

The authors acknowledge the support of the European Union's Horizon 2020 program, through a FET Open research and innovation action under Grant Agreements No. 899141 (PoLLoC) and No. 964770 (TopoLight). H.S. acknowledges

the Project No. 2022/45/P/ST3/00467 co-funded by the Polish National Science Centre and the European Union Framework Programme for Research and Innovation Horizon 2020 under the Marie Skłodowska-Curie Grant Agreement No. 945339.

-
- [1] F. Alet, A. M. Walczak, and M. P. Fisher, Exotic quantum phases and phase transitions in correlated matter, *Physica A* **369**, 122 (2006).
- [2] M. Greiner, O. Mandel, T. Esslinger, T. W. Hänsch, and I. Bloch, Quantum phase transition from a superfluid to a Mott insulator in a gas of ultracold atoms, *Nature (London)* **415**, 39 (2002).
- [3] L. Fallani, J. E. Lye, V. Guarrera, C. Fort, and M. Inguscio, Ultracold atoms in a disordered crystal of light: Towards a Bose glass, *Phys. Rev. Lett.* **98**, 130404 (2007).
- [4] I. Bloch, J. Dalibard, and S. Nascimbène, Quantum simulations with ultracold quantum gases, *Nat. Phys.* **8**, 267 (2012).
- [5] I. M. Georgescu, S. Ashhab, and F. Nori, Quantum simulation, *Rev. Mod. Phys.* **86**, 153 (2014).
- [6] D. Hanneke, J. P. Home, J. D. Jost, J. M. Amini, D. Leibfried, and D. J. Wineland, Realization of a programmable two-qubit quantum processor, *Nat. Phys.* **6**, 13 (2010).
- [7] M. Johanning, A. F. Varón, and C. Wunderlich, Quantum simulations with cold trapped ions, *J. Phys. B* **42**, 154009 (2009).
- [8] X. Peng, J. Zhang, J. Du, and D. Suter, Quantum simulation of a system with competing two- and three-body interactions, *Phys. Rev. Lett.* **103**, 140501 (2009).
- [9] R. Hanson and D. D. Awschalom, Coherent manipulation of single spins in semiconductors, *Nature (London)* **453**, 1043 (2008).
- [10] J. Q. You and F. Nori, Atomic physics and quantum optics using superconducting circuits, *Nature (London)* **474**, 589 (2011).
- [11] M. P. Harrigan, K. J. Sung, M. Neeley, K. J. Satzinger, F. Arute, K. Arya, J. Atalaya, J. C. Bardin, R. Barends, S. Boixo *et al.*, Quantum approximate optimization of non-planar graph problems on a planar superconducting processor, *Nat. Phys.* **17**, 332 (2021).
- [12] D. E. Chang, V. Vuletić, and M. D. Lukin, Quantum nonlinear optics—photon by photon, *Nat. Photon.* **8**, 685 (2014).
- [13] A. Periwal, E. S. Cooper, P. Kunkel, J. F. Wienand, E. J. Davis, and M. Schleier-Smith, Programmable interactions and emergent geometry in an array of atom clouds, *Nature (London)* **600**, 630 (2021).
- [14] S. Alyatkin, J. D. Töpfer, A. Askitopoulos, H. Sigurdsson, and P. G. Lagoudakis, Optical control of couplings in polariton condensate lattices, *Phys. Rev. Lett.* **124**, 207402 (2020).
- [15] S. Alyatkin, H. Sigurdsson, A. Askitopoulos, J. D. Töpfer, and P. G. Lagoudakis, Quantum fluids of light in all-optical scatterer lattices, *Nat. Commun.* **12**, 5571 (2021).
- [16] A. Kavokin, T. C. H. Liew, C. Schneider, P. G. Lagoudakis, S. Klemmt, and S. Hoefling, Polariton condensates for classical and quantum computing, *Nat. Rev. Phys.* **4**, 435 (2022).
- [17] Y. Zhang, X. Zhang, B. Tang, C. Tian, C. Xu, H. Dong, and W. Zhou, Realization of an all-optically controlled dynamic superlattice for exciton-polaritons, *Nanoscale* **10**, 14082 (2018).
- [18] L. Pickup, H. Sigurdsson, J. Ruostekoski, and P. G. Lagoudakis, Synthetic band-structure engineering in polariton crystals with non-Hermitian topological phases, *Nat. Commun.* **11**, 4431 (2020).
- [19] M. Pieczarka, E. Estrecho, S. Ghosh, M. Wurdack, M. Steger, D. W. Snoke, K. West, L. N. Pfeiffer, T. C. H. Liew, A. G. Truscott, and E. A. Ostrovskaya, Topological phase transition in an all-optical exciton-polariton lattice, *Optica* **8**, 1084 (2021).
- [20] J. D. Töpfer, I. Chatzopoulos, H. Sigurdsson, T. Cookson, Y. G. Rubo, and P. G. Lagoudakis, Engineering spatial coherence in lattices of polariton condensates, *Optica* **8**, 106 (2021).
- [21] N. G. Berloff, M. Silva, K. Kalinin, A. Askitopoulos, J. D. Töpfer, P. Cilibrizzi, W. Langbein, and P. G. Lagoudakis, Re-creating the classical XY Hamiltonian in polariton simulators, *Nat. Mater.* **16**, 1120 (2017).
- [22] J. Kasprzak, M. Richard, S. Kundermann, A. Baas, P. Jeambrun, J. M. J. Keeling, F. M. Marchetti, M. H. Szymańska, R. André, J. L. Staehli, V. Savona, P. B. Littlewood, B. Deveaud, and L. S. Dang, Bose-Einstein condensation of exciton polaritons, *Nature (London)* **443**, 409 (2006).
- [23] H. Ohadi, R. L. Gregory, T. Freegarde, Y. G. Rubo, A. V. Kavokin, N. G. Berloff, and P. G. Lagoudakis, Nontrivial phase coupling in polariton multiplets, *Phys. Rev. X* **6**, 031032 (2016).
- [24] J. D. Töpfer, H. Sigurdsson, L. Pickup, and P. G. Lagoudakis, Time-delay polaritonics, *Commun. Phys.* **3**, 2 (2020).
- [25] A. S. Abdalla, B. Zou, and Y. Zhang, Optical Josephson oscillation achieved by two coupled exciton-polariton condensates, *Opt. Express* **28**, 9136 (2020).
- [26] C. Domb and R. Potts, Order-disorder statistics IV. A two-dimensional model with first and second interactions, *Proc. R. Soc. London A* **210**, 125 (1951).
- [27] W. Selke, The ANNNI model—theoretical analysis and experimental application, *Phys. Rep.* **170**, 213 (1988).
- [28] M. Wolf and K. D. Schotte, Ising model with competing next-nearest-neighbour interactions on the kagome lattice, *J. Phys. A: Math. Gen.* **21**, 2195 (1988).
- [29] A. J. Ramírez-Pastor, F. Nieto, and E. E. Vogel, Ising lattices with $\pm J$ second-nearest-neighbor interactions, *Phys. Rev. B* **55**, 14323 (1997).
- [30] K. P. Kalinin, P. G. Lagoudakis, and N. G. Berloff, Exotic states of matter with polariton chains, *Phys. Rev. B* **97**, 161101(R) (2018).
- [31] K. P. Kalinin and N. G. Berloff, Computational complexity continuum within Ising formulation of NP problems, *Commun. Phys.* **5**, 20 (2022).
- [32] S. L. Harrison, H. Sigurdsson, S. Alyatkin, J. D. Töpfer, and P. G. Lagoudakis, Solving the max-3-cut problem with coherent networks, *Phys. Rev. Appl.* **17**, 024063 (2022).
- [33] C. Schneider, K. Winkler, M. D. Fraser, M. Kamp, Y. Yamamoto, E. A. Ostrovskaya, and S. Höfling, Exciton-polariton trapping and potential landscape engineering, *Rep. Prog. Phys.* **80**, 016503 (2017).

- [34] H. Deng, H. Haug, and Y. Yamamoto, Exciton-polariton Bose-Einstein condensation, *Rev. Mod. Phys.* **82**, 1489 (2010).
- [35] H. Yang and N. Y. Kim, Microcavity exciton-polariton quantum spin fluids, *Adv. Quantum Technol.* **5**, 2100137 (2022).
- [36] D. Read, T. C. H. Liew, Y. G. Rubo, and A. V. Kavokin, Stochastic polarization formation in exciton-polariton Bose-Einstein condensates, *Phys. Rev. B* **80**, 195309 (2009).
- [37] Y. del Valle-Inclan Redondo, H. Sigurdsson, H. Ohadi, I. A. Shelykh, Y. G. Rubo, Z. Hatzopoulos, P. G. Savvidis, and J. J. Baumberg, Observation of inversion, hysteresis, and collapse of spin in optically trapped polariton condensates, *Phys. Rev. B* **99**, 165311 (2019).
- [38] F. Meier and B. Zakharchenya, *Optical Orientation* (North Holland, Amsterdam, 1984), p. 523.
- [39] S. Pfalz, R. Winkler, T. Nowitzki, D. Reuter, A. D. Wieck, D. Hägele, and M. Oestreich, Optical orientation of electron spins in GaAs quantum wells, *Phys. Rev. B* **71**, 165305 (2005).
- [40] P. Renucci, T. Amand, X. Marie, P. Senellart, J. Bloch, B. Sermage, and K. V. Kavokin, Microcavity polariton spin quantum beats without a magnetic field: A manifestation of Coulomb exchange in dense and polarized polariton systems, *Phys. Rev. B* **72**, 075317 (2005).
- [41] A. Askitopoulos, A. V. Nalítov, E. S. Sedov, L. Pickup, E. D. Cherotchenko, Z. Hatzopoulos, P. G. Savvidis, A. V. Kavokin, and P. G. Lagoudakis, All-optical quantum fluid spin beam splitter, *Phys. Rev. B* **97**, 235303 (2018).
- [42] I. Gnusov, H. Sigurdsson, S. Baryshev, T. Ermатов, A. Askitopoulos, and P. G. Lagoudakis, Optical orientation, polarization pinning, and depolarization dynamics in optically confined polariton condensates, *Phys. Rev. B* **102**, 125419 (2020).
- [43] I. Gnusov, H. Sigurdsson, J. D. Töpfer, S. Baryshev, S. Alyatkin, and P. G. Lagoudakis, All-optical linear-polarization engineering in single and coupled exciton-polariton condensates, *Phys. Rev. Appl.* **16**, 034014 (2021).
- [44] L. Pickup, J. D. Töpfer, H. Sigurdsson, and P. G. Lagoudakis, Polariton spin jets through optical control, *Phys. Rev. B* **103**, 155302 (2021).
- [45] G. Panzarini, L. C. Andreani, A. Armitage, D. Baxter, M. S. Skolnick, V. N. Astratov, J. S. Roberts, A. V. Kavokin, M. R. Vladimirova, and M. A. Kaliteevski, Cavity-polariton dispersion and polarization splitting in single and coupled semiconductor microcavities, *Phys. Solid State* **41**, 1223 (1999).
- [46] E. Kammann, T. C. H. Liew, H. Ohadi, P. Cilibrizzi, P. Tsotsis, Z. Hatzopoulos, P. G. Savvidis, A. V. Kavokin, and P. G. Lagoudakis, Nonlinear optical spin Hall effect and long-range spin transport in polariton lasers, *Phys. Rev. Lett.* **109**, 036404 (2012).
- [47] C. Antón, S. Morina, T. Gao, P. S. Eldridge, T. C. H. Liew, M. D. Martín, Z. Hatzopoulos, P. G. Savvidis, I. A. Shelykh, and L. Viña, Optical control of spin textures in quasi-one-dimensional polariton condensates, *Phys. Rev. B* **91**, 075305 (2015).
- [48] A. Kavokin, G. Malpuech, and M. Glazov, Optical spin Hall effect, *Phys. Rev. Lett.* **95**, 136601 (2005).
- [49] C. Leyder, M. Romanelli, J. P. Karr, E. Giacobino, T. C. H. Liew, M. M. Glazov, A. V. Kavokin, G. Malpuech, and A. Bramati, Observation of the optical spin Hall effect, *Nat. Phys.* **3**, 628 (2007).
- [50] M. Maragkou, C. E. Richards, T. Ostatnický, A. J. D. Grundy, J. Zajac, M. Hugues, W. Langbein, and P. G. Lagoudakis, Optical analogue of the spin Hall effect in a photonic cavity, *Opt. Lett.* **36**, 1095 (2011).
- [51] K. Y. Bliokh, F. J. Rodríguez-Fortuño, F. Nori, and A. V. Zayats, Spin-orbit interactions of light, *Nat. Photonics* **9**, 796 (2015).
- [52] K. Lekenta, M. Król, R. Mirek, K. Łempicka, D. Stephan, R. Mazur, P. Morawiak, P. Kula, W. Piecek, P. G. Lagoudakis, B. Piętka, and J. Szczytko, Tunable optical spin Hall effect in a liquid crystal microcavity, *Light Sci. Appl.* **7**, 74 (2018).
- [53] K. Łempicka-Mirek, M. Król, H. Sigurdsson, A. Wincukiewicz, P. Morawiak, R. Mazur, M. Muszyński, W. Piecek, P. Kula, T. Stefaniuk, M. Kamińska, L. De Marco, P. G. Lagoudakis, D. Ballarini, D. Sanvitto, J. Szczytko, and B. Piętka, Electrically tunable Berry curvature and strong light-matter coupling in liquid crystal microcavities with 2D perovskite, *Sci. Adv.* **8**, eabq7533 (2022).
- [54] D. Aristov, H. Sigurdsson, and P. G. Lagoudakis, Screening nearest-neighbor interactions in networks of exciton-polariton condensates through spin-orbit coupling, *Phys. Rev. B* **105**, 155306 (2022).
- [55] See Supplemental Material at <http://link.aps.org/supplemental/10.1103/PhysRevB.108.L161301> for additional information on experimental details, TE-TM splitting and real space distribution of S_z component of the stokes vector from a single isolated polariton condensate; two dimensional spinor polariton model; theory of the threshold behaviour in a spin screened condensate triad; comparison with RKKY mechanism and discussion on the potential generation of spinor polariton vortical array, which also includes Refs. [56,57,59].
- [56] M. Z. Maialle, E. A. de Andrada e Silva, and L. J. Sham, Exciton spin dynamics in quantum wells, *Phys. Rev. B* **47**, 15776 (1993).
- [57] V. Savona, Effect of interface disorder on quantum well excitons and microcavity polaritons, *J. Phys.: Condens. Matter* **19**, 295208 (2007).
- [58] P. Cilibrizzi, A. Askitopoulos, M. Silva, F. Bastiman, E. Clarke, J. M. Zajac, W. Langbein, and P. G. Lagoudakis, Polariton condensation in a strain-compensated planar microcavity with InGaAs quantum wells, *Appl. Phys. Lett.* **105**, 191118 (2014).
- [59] M. A. Ruderman and C. Kittel, Indirect exchange coupling of nuclear magnetic moments by conduction electrons, *Phys. Rev.* **96**, 99 (1954).